FLUCTUATION AND LINEAR ANALYSIS OF Na-CURRENT KINETICS IN SQUID AXON

HARVEY M. FISHMAN, H. RICHARD LEUCHTAG, AND L. E. MOORE
Department of Physiology and Biophysics, University of Texas Medical Branch, Galveston, Texas 77550

ABSTRACT The power spectrum of current fluctuations and the complex admittance of squid axon were determined in the frequency range 12.5 to 5,000 Hz during membrane voltage clamps to the same potentials in the same axon during internal perfusion with cesium. The complex admittance was determined rapidly and with high resolution by a fast Fourier transform computation of the current response, acquired after a steady state was attained, to a synthesized signal with predetermined spectral characteristics superposed as a continuous, repetitive, small perturbation on step voltage clamps. Linear conduction parameters were estimated directly from admittance data by fitting an admittance model, derived from the linearized Hodgkin-Huxley equations modified by replacing the membrane capacitance with a "constant-phase-angle" capacitance, to the data. The constant phase angle obtained was ~81°. At depolarizations the phase of the admittance was 180°, and the real part of the impedance locus was in the left-half complex plane for frequencies below 1 kHz, which indicates a steady-state negative Na conductance. The fits also yielded estimates of the natural frequencies of Na "activation" and "inactivation" processes. By fitting Na-current noise spectra with a double Lorentzian function, a lower and an upper corner frequency were obtained; these were compared with the two natural frequencies determined from admittance analysis at the corresponding potentials. The frequencies from fluctuation analyses ranged from 1.0 to 10.3 times higher than those from linear (admittance) analysis. This discrepancy is consistent with the concept that the fluctuations reflect a nonlinear rate process that cannot be fully characterized by linear perturbation analysis. Comparison of the real part of the admittance and the current noise spectrum shows that the Nyquist relation, which generally applies to equilibrium conductors, does not hold for the Na process in squid axon. The Na-channel conductance, γ_{Na}, was found to increase monotonically from 0.1 to 4.8 pS for depolarizations up to 50 mV from a holding potential of −60 mV, with no indication of a maximum value.

INTRODUCTION

In the classification and analysis of any process the questions of whether it can be validly described by equilibrium concepts and whether linear mathematics are sufficient are foremost, because of their profound implications on the choice of a body of physical theory to bring to bear on the process for its quantitative description. Prevailing models of ion conduction in cell membranes, in particular, nerve membranes, assume equilibrium processes and linear rate theory or simple extensions to obtain nonlinear descriptions, notwithstanding the fact that conduction in these membranes is driven by electrochemical gradients, and that a quantitative test of the assumption of linear kinetics at the microscopic level has not previously been made.

With the development and refinement in the techniques for recording and analyzing membrane current fluctuations, it is possible to obtain accurate information on the microscopic nature of conduction processes in membranes. Currently the focus of most noise studies is the calculation of single ion-channel conductances, based on simplifying assumptions about the conduction process. While these calculations are useful, it should not be forgotten that fluctuation analysis can also yield additional information of a general nature, independent of the model used.

In this paper we examine the spectral properties of the Na-conduction system in squid axon and their implications to the applicability of equilibrium and linear kinetics to this system. In addition to these fluctuation measurements and analyses, we obtain a linear description of Na conduction directly from measurements of the complex admittance using small-amplitude (≈1 mV peak-to-peak) pseudorandom perturbations during step voltage clamps and the subsequent fitting of a linear model to these data. The noise and admittance data, obtained on the same axons under the same conditions, were found to yield significantly different values for kinetic parameters of Na conduction. This finding indicates that the microscopic kinetics of the Na-current process are nonlinear and hence are not adequately characterized by linear perturbation analysis.

A comparison of the observed power spectrum with that derived from the measured admittance by means of the Nyquist (1928) relation shows that Na-conduction noise exceeds the Nyquist prediction. Furthermore, calculations of the single Na-channel conductance from these data show a voltage dependency for this parameter, which is

indicative of a multiconductance channel. A preliminary report of this work has been published (Fishman et al., 1982).

METHODS

Preparation and Solutions

The axons used in these experiments, from the hindmost stellar nerve of the squid *Loligo pealei*, were obtained at the Marine Biological Laboratory in Woods Hole, MA. A 3-cm length of axon was removed from an animal and threaded through 0.6-mm diameter holes in two thin (0.1 mm) Mylar partitions, spaced 5-mm apart, which formed the central compartment, through which cooled, artificial sea water (ASW) flowed. Vaseline was applied to the partition holes before and after threading the axon to electrically isolate the ends. On both sides of the central compartment the axon extended into an air gap (6 mm in length) and rested on a plastic support. The axon was held taut, but not stretched, by pushing the threads at the tied-off ends into sticky wax at the base of each support. The central compartment contained a thermocouple probe for temperature measurement. A platinized platinum sheet, 4 mm × 4 mm, was used as the external current electrode and a chlorided silver wire in an ASW-filled glass capillary was used for external potential measurement. The external solution was an ASW composed of 430 mM NaCl, 10 mM KCl, 10 mM $CaCl_2$, 5 mM Tris · Cl. The internal perfusate consisted of 0.3 M CsF, 0.39 M sucrose buffered to pH 7.4 at 22°C with 5 mM Tris · Cl.

Improvements in the Axial-Electrode Voltage Clamp

Low Voltage-Noise Primary Stage. In a conventional internal axial-electrode voltage clamp of a squid axon, the current is usually measured from a membrane area of ~0.2 cm^2, which has an impedance at 10 Hz under standard ionic conditions of 3–5 kΩ at rest potential. This low impedance results in substantial background noise from the clamp system because of the much larger sources of noise (thermal and other) introduced into the measurement of transmembrane voltage by the impedance of the internal potential-sensing electrode (typically 100 kΩ) as well as by the subsequent electronics.

Low voltage-noise performance (10–15 $nV/\sqrt{Hz}$) can be obtained from an amplifier when it is driven from source impedances of ~1 MΩ (Fishman et al., 1975 *a*). Since the typical area of squid axon used yields a much lower impedance, as mentioned above, it is necessary to reduce the background voltage-noise produced by the voltage-sensing electrodes and subsequent instrumentation to attain improvements in the noise performance of an axial-electrode clamp.

To obtain a low-noise amplifier (LNA) suitable for an axial-electrode clamp of squid axon, several discrete operational amplifiers in parallel have been used previously to reduce the intrinsic voltage-noise density by $1/\sqrt{n}$, where n is the number of paralleled amplifiers (DeFelice et al., 1975; Fishman et al., 1981). However, the size and cost of the combined amplifiers becomes prohibitive, especially in the case of a differential amplifier, which requires twice as many devices. A recent design by Dr. T. Iwazumi (University of Texas, Galveston, TX) of a new primary stage to the clamp system, which uses a dual field-effect transistor (FET) (2SK146, Toshiba International Corporation, San Francisco, CA) containing 100 FET (50 paralleled on each side for differential operation) in a single device, has solved this problem.

The circuit shown in Fig. 1 is used as the primary voltage-sensing stage of an otherwise conventional clamp system. A gain of 100 (at a bandwidth of 1 MHz) in this stage makes the noise from subsequent stages relatively insignificant. Fig. 2 shows that the measured voltage-noise density (referred to input) with short-circuited input decreases from 2 to 1 $nV/\sqrt{Hz}$ in the frequency range 20–1,000 Hz, which corresponds to an equivalent thermal noise of a 200–100-Ω resistor. When the input is terminated with a 1 kΩ resistor, the voltage-noise density (Fig. 2) is nearly equal to the theoretical value (4 $nV/\sqrt{Hz}$) in the 20–1,000 Hz range. Thus with this stage the voltage noise from the clamp electronics is insignificant with respect to the noise from the voltage-sensing electrodes.

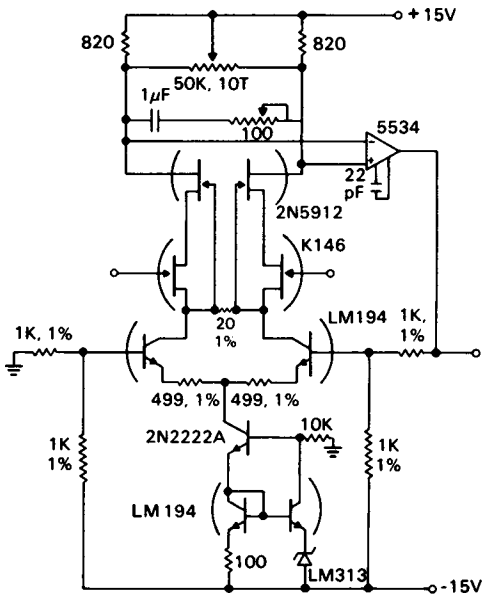

FIGURE 1 Circuit of the primary voltage-sensing stage used in squid-axon voltage-clamp measurements. Designed by Dr. T. Iwazumi, this low-noise stage uses a Toshiba 2SK146 device (Toshiba International Corporation), containing 50 field-effect transistors (FET) in parallel on each side of the differential configuration to reduce the intrinsic voltage-noise density as a function of frequency by a factor of 0.14 of that obtained by use of a single FET on each side. Resistances in ohms.

Reduction of the Noise and Impedance of the Internal Potential Pipette. After elimination of the clamp electronics as a significant source of background noise, the next component of the system that required improvement was the internal potential pipette. The usual

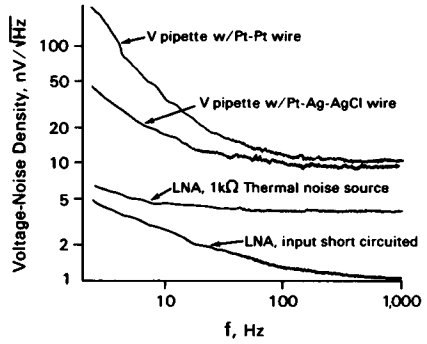

FIGURE 2 Voltage-noise density of the LNA shown in Fig. 1. The intrinsic voltage noise of the LNA with short-circuited input is equivalent to the thermal noise of a 100–200 Ω resistor in the range 10–1,000 Hz. With the input terminated with a 1 kΩ resistor, the measured noise is very close to the theoretical thermal noise (4 $nV/\sqrt{Hz}$). Thus the LNA introduces negligible noise into the clamp measurement relative to electrode noise. The major source of background noise introduced into the clamp comes from the internal axial voltage-sensing pipette (shown in inset of Fig. 3), which was measured for two different plated wires extending out of the tip.

internal, axial pipette has a bare Pt wire within the capillary. A significant decrease of the pipette impedance can be obtained by using a platinized platinum (Pt-Pt) wire instead of a bare Pt wire (Fishman, 1973). Further reduction in pipette impedance can be obtained if the Pt-Pt wire extends 200–300 μm out of the tip. This can be seen in Fig. 3, where the complex impedance of the extended wire capillary is shown. The decreased impedance is due to a shunting, by the wire, of the spreading resistance at the tip of the pipette, which sets a lower limit on the pipette impedance when the wire does not extend beyond the tip. An additional decrease in impedance, particularly at frequencies below 100 Hz, is obtained by using an extended platinized, silver silver-chloride (Pt-Ag-AgCl) wire of the type described by Cole and Kishimoto (1962). Fig. 3 shows the impedance magnitude of the latter to be 5 kΩ in the range 10 Hz to 10 kHz. The voltage-noise density of the extended-wire pipette with Pt-Pt and Pt-Ag-AgCl wires is shown in Fig. 2. The figure shows that as the impedance of the pipette is decreased the voltage noise decreases. These measurements, made with the LNA, show that the major source of voltage noise is due to the internal voltage electrode. Although this noise source is reduced considerably by use of the Pt-Ag-AgCl extended wire, it nevertheless contributes 10 nV/$\sqrt{\text{Hz}}$ at 1 kHz and requires correction (see below) in power spectra in which spectral form is important at 1 kHz and above (e.g., Na noise).

A disadvantage of the Pt-Ag-AgCl extended wire pipette is that the direct current (dc) potential derived from it contains a junction potential that is difficult to assess, particularly when the ionic composition of the internal perfusate is changed. Estimates of this offset potential can be obtained by placing the pipette in solutions of the various perfusates used. For CsF perfusates this offset was in the range 10–30 mV. In separate experiments with a conventional internal pipette to measure transmembrane potential, the admittance was found to be a sensitive indicator of this potential within a few millivolts. This property was used to estimate the absolute membrane potentials given in the present experiments. Another aberration associated with this electrode is due to polarization effects. These can be kept to a minimum by using a period of 10 s or more between application of successive clamp steps.

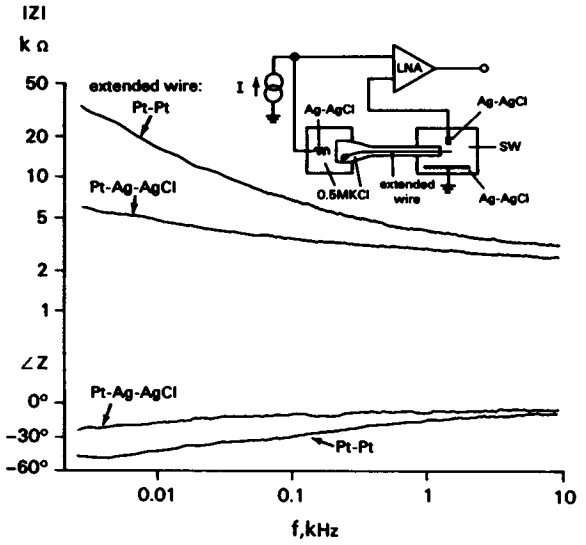

FIGURE 3 Magnitude and phase plots of the impedance of the internal axial voltage electrode under two conditions. The impedance is reduced by using a floating, Pt-Pt wire instead of a bare Pt wire within the capillary and by extending the tip of the wire 0.2–0.3 mm beyond the pipette (Fishman, 1973). Further reduction in low-frequency impedance is obtained by use of a platinized, silver silver-chloride wire, as described by Cole and Kishimoto (1962). The impedance decrease is accompanied by a decrease in the voltage noise, as shown in Fig. 2. Precautions must be taken to minimize offset and polarization effects.

Current Measurements. The use of either the Marmont (1949) externally guarded current technique or the alternative differential measurement scheme of Hodgkin et al. (1952) creates a very noisy condition (Fishman, 1982). In the Marmont method, the resistance from guard to central current electrode is ~10Ω without partitions and is difficult to raise beyond 1 kΩ with partitions and Vaseline seals. This low interelectrode resistance is the source resistance for the operational amplifier measuring the virtual-ground current, and results in a current-noise density of 3 nA/$\sqrt{\text{Hz}}$. Since axon current-noise density is typically 0.1 nA/$\sqrt{\text{Hz}}$, this is an intolerable condition. Consequently, the guards were removed to eliminate the low-impedance input shunt of the virtual-ground amplifier and to restore good noise performance to the current measurement. To minimize distortion of the central current measurement by axon-end effects, partitions and Vaseline seals were retained. Although there were occasional "notches" in usual step-clamp currents at low voltages, this was the best available compromise. Furthermore, whenever these aberrations appeared in admittance measurements as changes in the admittance determinations for successively applied perturbations, the affected data were rejected. Deactivation of the ends by heat treatment with a hot nichrome wire has been useful, but after such treatment the apparent leakage increases due to the shunt of the "dead" ends on the central length of axon. The shunt is ohmic and can be taken into account during curve fitting as a voltage-independent element at hyperpolarized potentials.

Noise and Admittance Measurements on the Same Axon

Fourier Synthesized Pseudorandom Signal (FSPS). An essential requirement of the measurements in these experiments is that both noise and admittance data be obtained on the same axon under the same conditions. To achieve this objective, efficient use of experimental time is necessary. During the past five years, we have developed a hybrid system (combination of hard-wired instrumentation and computer) for this purpose. The details of this system have appeared in several publications (Fishman et al., 1979, 1981; Poussart and Ganguly, 1977). For brevity we focus on recent improvements.

A synchronized, pseudorandom signal (PS) has several distinct features that permit rapid transfer function analysis. It is deterministic; that is, its frequency domain properties (real and imaginary parts) are fixed. For a particular signal, its real and imaginary parts need only be determined once through a fast Fourier transform (FFT) calculation, and they remain the same as long as that particular signal is used as the perturbation function to the clamp system. By synchronizing the PS with the "clock" (repetitive pulse train) that runs the analog-to-digital (A/D) converter of an FFT processor, the complex values of the frequency components in the waveform become independent of the clock frequency. That is, the spectral intensity of each frequency component and their distribution (spectral form) remain constant while the frequency of each of the components is determined by the clock frequency. Thus the PS has the same fixed spectral properties in any frequency range, which is determined solely by the frequency of the clock that runs the A/D converter. The pseudorandom character of the time waveform produces a high density of frequency components in any given frequency range, which provides excellent resolution of a transfer function.

We have implemented a new type of PS that is synthesized through specification of its complex spectral form (Fishman et al., 1981). The analytical expression for the time-domain function consists of a sum of 400 sinusoidal components with amplitudes that produce a desired spectral form and a random phase angle associated with each frequency component. This time waveform was computed by an inverse FFT of the specified spectral form with different sets of random phases. A waveform that had minimum peak-to-peak excursion was chosen to minimize excursions of the voltage when the waveform was used as a command to the clamp system. Each of 1,024 equally spaced digital values of the selected-time waveform is permanently stored in a read-only memory (ROM). When used as a clamp perturbation, this Fourier-synthesized

pseudorandom signal (FSPS) is clocked out of the ROM by the sample clock of the A/D converter of the Fourier processor and converted to analog form.

Several important advantages result from the use of the FSPS instead of the pseudorandom binary signal (PRBS) used previously. The ROM contains information required for four FSPS, each of which approximates the inverse spectral property of the axon response under a different experimental condition. Thus the use of these spectrally shaped waveforms results in a prewhitening of the response, which significantly reduces errors due to the finite dynamic range of the digital-signal processing section during the data acquisition. In fact, without use of these prewhitened signals the dynamic range of the squid axon admittance would preclude, in many instances, a single-shot determination of the admittance due to large uncertainties in spectral estimates in a substantial portion of the analysis range. Furthermore, synchronization is simplified by direct use of the sample clock of the A/D converter. With the PRBS method, the period of the PRBS must be precisely matched to the duration of the time window of the FFT sampling (Poussart and Ganguly, 1977), which requires a separate 10-MHz master clock and a practical limit to frequency analysis of 10 kHz or less. With the FSPS the upper frequency limit of a measurement is dependent only on the highest frequency of operation of the A/D converter, which is 256 kHz in our system.

An admittance determination is made by first storing the real (Re) and imaginary (Im) parts of the FSPS by inputing the digital-to-analogue (D/A) version of the waveform through an anti-alias filter (elliptic 120 dB/oct) matched to the frequency-analysis band. Thereafter the current response of the axon during a clamp step with superposed FSPS as a small ($\approx$1 mV peak-to-peak) perturbation is processed through the same anti-alias filter. The Re and Im parts are then determined, and the admittance (complex ratio of current to voltage) is computed and displayed as Bode (magnitude and phase vs. frequency) plots or a complex (Re vs. Im) plane plot. The complex admittance is then stored on floppy disk for later retrieval for model curve fitting. A microprocessor-based sequencer has been designed to allow the admittance to be determined at arbitrary times after the application of a step clamp. In the case of acquisition of spontaneous current noise data during a step clamp, the FSPS is not applied to the clamp, and the same procedure is used as in the admittance case, but with more gain in the signal-processing path.

Coherence Elimination Method. A significant problem in the analysis of admittance or noise data, derived during a clamp step, arises from slow variations in the mean current during the acquisition interval. Changes in the mean current introduce contaminating spectral components and cause errors in the spectral estimates. To eliminate these errors, a method of removing slow variations of the mean current from the response to a FSPS or the spontaneous current noise was developed (Fishman et al., 1981). First the mean-current pedestal (dc offset) on which the response to an applied FSPS occurs or about which the current noise occurs is removed with a simple, passive high-pass filter prior to amplification to maximize dynamic range. In the case of an admittance measurement the polarity of a small amplitude FSPS, which is superposed on the step-clamp command, is alternately changed (toggled) with each successively applied step clamp. The high-pass filtered, amplified current, I_M, in response to the first step clamp is digitized at the desired time interval during the first step and placed in memory A. The polarity of the FSPS is changed prior to application of the second step clamp and the procedure repeated with the digital values of the response placed in another memory, B. Immediately after memory B has been loaded, a digital subtraction is performed between the corresponding digital values in memory A and those of memory B, and the resulting digital sequence is then converted to analog form and applied to the Fourier processor for analysis. A similar method was used by Conti et al. (1980).

Usually the admittance is obtained from the response to a single pair of FSPS-superposed step-clamp pulses, and there is no need for further data unless the average of several admittance determinations is desired. The toggled FSPS makes the response that carries the admittance during any successive pair of step clamps incoherent, so that they will add, whereas the mean current, if invariant from step to step, will be coherent and removed from the digital-data sequence. In the case of noise measurements, the FSPS is not applied and the digital values in memory reflect both the fluctuations, which are incoherent with respect to each applied pulse, and the mean current, which is coherent. The pairwise subtraction effectively eliminates the mean-current variation from the digital-data sequence upon which an FFT is calculated so that slow changes in the mean current are tracked in time to produce less spectral distortion.

Spectral Corrections. Since high-pass filtering of the noise or FSPS response waveform is used in the acquisition of data during a step clamp, spectral corrections for this and other distortions due to processing instrumentation must be made. In the noise measurement mode, the passband characteristic (magnitude-squared transfer function) of the signal-processing path from the clamp system to the FFT processor is obtained and stored. Each average power spectrum generated from the acquired noise data is software corrected for this passband characteristic of the signal-processing instrumentation before display and storage. In addition, in the admittance measurements, instead of using the FSPS as the reference for the transfer function calculation, the response obtained from a voltage clamp of a resistor (1 kΩ) substituted for the preparation is used. The latter contains the overall complex passband characteristic of the signal-processing instrumentation, which is automatically removed in the transfer function (ratio) computation because it is common to both reference and response functions.

Determination and Removal of Background Current Noise. As mentioned earlier, the voltage-sensing electrodes produce significant background voltage noise (particularly above 1 kHz), which is converted to a background current noise by multiplying by the absolute square of the admittance of the axon. To verify that electrode noise is the major source of background noise, we calculated a background current-noise spectrum from the voltage noise of the voltage-sensing electrodes determined on the preparation at an absolute membrane potential of -80 mV, where voltage-dependent Na conductance was negligible. The calculated background noise in the frequency range 800–5,000 Hz at hyperpolarized potential matched the current-noise power spectrum from the axon measured at the same potential, confirming that the electrode noise applied to membrane admittance accounts for the background at the upper spectral range. The spectrum of the background current noise was therefore obtained and subtracted from the stored raw current-noise spectrum at each membrane potential in the following manner. As shown in Fig. 4, the voltage noise power spectrum, S_V, of the voltage-sensing electrodes and primary stage (low noise) amplifier is determined in each frequency analysis range and stored. From the stored admittance data, the squared magnitude of the axon admittance, $|Y|^2$, is computed at each potential in the same frequency range. A background current-noise power spectrum is computed as $S_{IB} = S_V |Y|^2$ for each potential, as shown in Fig. 4. The background spectrum is then subtracted from the stored, raw current-noise spectrum, S_I (obtained at the same potential as the admittance) to produce the current-noise spectrum (in the case shown, $S_{I_{Na}}$) with the background spectrum removed. This is a crucial correction for model fitting and parameter estimation of the Na system, because the spectral form for frequencies above 800 Hz cannot be determined accurately without this correction. Compare the spectra in Fig. 5, which are not corrected for background noise, with the spectra in Fig. 9, which are corrected.

Series Resistance Compensation

To mitigate errors in membrane voltage during step clamps, the series resistance, R_S, between the internal and external voltage electrodes and the membrane was measured and compensated by current feedback to the control amplifier of the voltage-clamp system (Hodgkin et al., 1952). A separate wideband current source driven by a small amplitude FSPS (see Noise and Admittance Measurements on the Same Axon section) and a

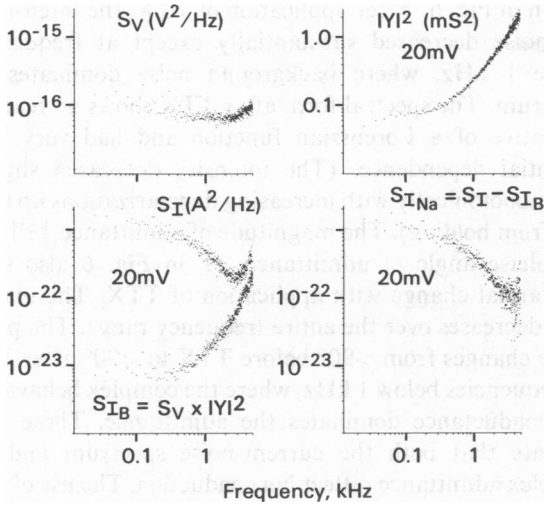

FIGURE 4 Example of the correction of an Na current-noise spectrum for background noise. The voltage-noise spectrum, S_V, due to the voltage-sensing electrodes (*upper left*) is multiplied by the square of the membrane admittance magnitude spectrum, $|Y|^2$ (*upper right*), measured at a particular clamp voltage (20 mV in this case) to obtain the background current-noise spectrum, S_{I_B}, shown together with the uncorrected current-noise spectrum, S_I, (also measured at 20 mV) in the *lower left*. The corrected noise spectrum, $S_{I_{Na}} = S_I - S_{I_B}$, ready for fitting, is shown at the *lower right*.

voltage-recording stage were used to measure the membrane complex impedance between internal and external voltage electrodes. The impedance measurements were made at hyperpolarized potential to minimize membrane conductance in the frequency range 250 Hz to 100 kHz. The series resistance was estimated by extrapolation of the complex-plane impedance locus to infinite frequency to obtain the point of intersection with the real axis. For the ionic conditions of internal Cs perfusion and ASW externally, R_S determinations ranged from 3.6 to 3.9 $\Omega \cdot cm^2$.

Model Testing and Data Fitting

To obtain quantitative information from the admittance and noise data, models of the ion-conduction processes were compared with the data. This was done by two separate curve-fitting programs in which a model could be specified and the fitting was done by the method of least squares. One of these minimizes the chi-square with respect to each model parameter separately (grid search), and the other, with respect to all the parameters simultaneously (gradient search) (Bevington, 1969). These programs were tested extensively by generating computational data from analytical functions and entering them into the programs to ascertain the goodness of fit, parameter estimates, and susceptibility to false minima. By alternate use of grid and gradient searches, and by fitting with a variety of initial estimates, the problem of false minima could be overcome.

The admittance model contains eight parameters and is equivalent to the linearized Hodgkin-Huxley admittance with a series resistance and a constant-phase-angle capacitance (Cole and Cole, 1941) to take into account the nonideal properties of membrane capacitance. To reduce the number of independent parameters in the curve fits from 8 to 5, high-frequency (100-kHz band) impedance measurements were made (Leuchtag et al., 1982) to obtain a better characterization of the membrane capacitance and the series access impedance. In the range 10–100 kHz, the axon impedance is voltage-independent, passive, and dominated by these two phenomenological processes. The independent characterization of these makes it possible to fit the low-frequency data with fewer degrees of freedom, thus eliminating possible ambiguities.

The model in the curve-fitting program of power spectra consisted of any combination of white (A_0), pink (A/f), or sum of Lorentzian ($A_1/[1 + (f/\nu_1)^2] + A_2/[1 + (f/\nu_2)^2]$) functions. From model fits of admittance and noise spectra over a wide range of membrane voltage, the following information is obtained: (*a*) the natural frequencies (f_1 and f_2) of the linearized system, (*b*) the corner frequencies (ν_1 and ν_2) of noise spectral components, (*c*) the intensity and form of noise spectra, (*d*) the Nyquist prediction for the noise spectra, (*e*) the linearized conduction parameters, and (*f*) the current-noise variance. Comparison of *a* and *b* indicates whether the kinetics of the ion channels examined are linear or nonlinear. This comparison yields the desired information because the fluctuations reflect the microscopic character of the (linear or nonlinear) kinetics of conduction directly, whereas the admittance reflects only the linear part of the behavior of the microscopic system (van Kampen, 1969). Macroscopic linearity, therefore, is not necessarily due to microscopic linearity; it can also be due to cancellation of nonlinear terms when averaging over a large number of entities. Comparison of *c* and *d* provides additional information on the elementary conduction process because the Nyquist relation gives the theoretical noise of a linear conducting system that is in equilibrium. Given that current noise is expected to be

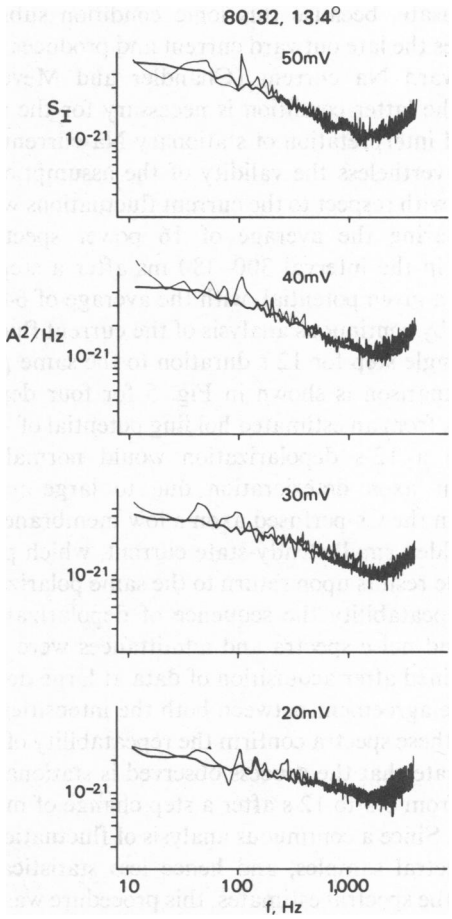

FIGURE 5 Test for stationarity of Na-current fluctuations. Spectral pairs at the same potential were obtained in two ways. (*a*) A spectrum was obtained from the fluctuations recorded in the interval 300–380 ms after a step clamp. 16 such spectra generated in the same interval during 16 step clamps to the same potential were averaged to give an averaged spectrum (light lines, ——) at each indicated step potential. (*b*) An average of 64 spectra was obtained over a 12-s interval (heavy lines, ——) by continuous analysis of fluctuations after a single step to each of the same potentials. Potentials shown are steps from an estimated holding of −60 mV. The agreement between the pairs of spectra indicates that the data are stationary over the 0.3–12-s interval. The spectra are not corrected for background noise, which becomes significant above 1 kHz.

dominated by nonequilibrium excess noise due to ion movements through channels triggered by their openings and closings, this comparison may seem trivial. However there are instances where the Nyquist relation is approximately valid for a nonequilibrium process (see Fig. 6, Frehland and Faulhaber, 1980). From *e* and *f* and a measure of the reversal potential, the single-channel conductance can be computed as a function of voltage to ascertain whether the elementary process has one or more conducting states.

RESULTS

Comparison of Power Spectra of Fluctuations Obtained during Short Step Clamps with those Obtained during Steady State

We chose to study the Na-current system under internal perfusion, with cesium ion replacing all of the potassium in the perfusate, because this ionic condition substantially suppresses the late outward current and produces a steady-state inward Na current (Chandler and Meves, 1965, 1970). The latter condition is necessary for the measurement and interpretation of stationary Na-current fluctuations. Nevertheless the validity of the assumption of stationarity with respect to the current fluctuations was tested by comparing the average of 16 power spectra, each obtained in the interval 300–380 ms after a step voltage clamp to a given potential, with the average of 64 spectra, obtained by continuous analysis of the current fluctuations after a single step for 12 s duration to the same potential. This comparison is shown in Fig. 5 for four depolarized potentials from an estimated holding potential of −60 mV. Although a 12-s depolarization would normally cause significant axon deterioration due to large membrane current, in the Cs-perfused axon a low membrane conductance yielded small steady-state current, which permitted repeatable results upon return to the same polarization. To assure repeatability the sequence of depolarizations was varied, and noise spectra and admittances were routinely redetermined after acquisition of data at large depolarizations. The agreement between both the intensities and the forms of these spectra confirm the repeatability of the data and indicate that the process observed is stationary in the interval from 0.3 to 12 s after a step change of membrane potential. Since a continuous analysis of fluctuations yields more spectral samples, and hence less statistical uncertainty in the spectral estimates, this procedure was adopted in the analysis of all subsequent noise data.

Identification of Na-Conduction Noise and Admittance

To establish that the noise spectra and admittances reflect essentially voltage-dependent Na conduction, tetrodotoxin (TTX) (10^{-6}M) was added to the external ASW to eliminate Na current. A representative set of these data obtained at the same membrane potential (30 mV depolarized from a holding of −60 mV) and in the same axon are shown in Fig. 6. After application of TTX, the intensity of the noise decreased substantially except at frequencies above 1 kHz, where background noise dominates the spectrum. The spectral form after TTX shows no features indicative of a Lorentzian function and had very little potential dependence. (The intensity decreased slightly and monotonically with increasing depolarizations up to 50 mV from holding). The magnitude of admittance, $|Y|$, and the phase angle of admittance, $\angle Y$ in Fig. 6 also show substantial change with application of TTX. The magnitude decreases over the entire frequency range. The phase angle changes from >90° before TTX to <90° after TTX at frequencies below 1 kHz, where the complex behavior of Na conductance dominates the admittance. These data indicate that both the current-noise spectrum and the complex admittance reflect Na conduction. The use of 50%

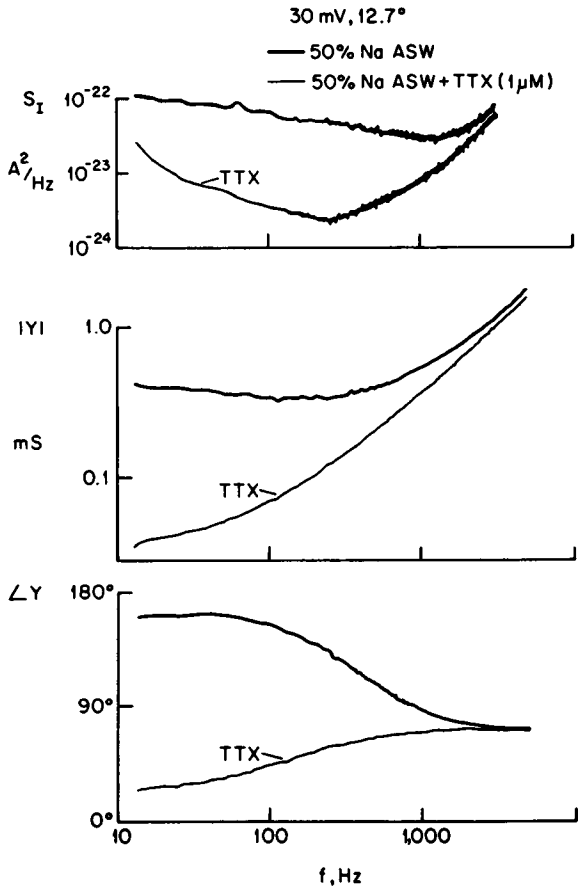

FIGURE 6 Noise power spectrum S_I, magnitude, $|Y|$, and phase angle, $\angle Y$, of complex admittance before and after TTX at a 30-mV depolarization from holding potential (−60 mV). All data from the same axon. Axon area ~0.05 cm². Note that suppression of Na conduction with TTX substantially alters both S_I and $Y(j\omega)$, indicating that Na conduction is reflected in both measurements. Because $Y(j\omega)$ is altered after TTX, the background noise evident in S_I above 800 Hz (before TTX) is not properly removed by subtraction of S_I after TTX. Instead the procedure illustrated in Fig. 4 must be used. Each noise spectrum is an average of 128 individual spectra acquired in a 24-s interval after a 30 mV step clamp. The admittance data were acquired in an 80 ms interval 1 s after a 30-mV step clamp.

Na ASW to obtain the data in Fig. 6 mitigates the observations that are described above; the differences before and after TTX with full Na ASW are even greater than those shown.

Determination and Removal of Background Noise to Obtain Na-Noise Spectrum

Because of the substantial alteration of the complex admittance after suppression of Na conduction with TTX, shown in Fig. 6 at a depolarized potential and previously at rest potential (Fishman et al., 1979), the use of spectra in TTX to correct for background noise is precluded. A more accurate correction of noise spectra for background current noise is obtained by use of the procedure illustrated in Fig. 4. For example, referring to Fig. 6, at 1 kHz $|Y|$ is 0.53 mS before TTX and 0.36 mS after TTX. If the noise power spectrum after TTX is assumed to be background noise, at 1 kHz the power density is 0.83×10^{-23} A^2/Hz. However, the actual background spectral density at 1 kHz is 1.2×10^{-23} A^2/Hz, computed from the relation $S_{I_b} = S_V|Y|^2$, where S_V is the voltage-noise power density of voltage electrodes and subsequent instrumentation (4.3×10^{-17} V^2/Hz at 1 kHz), and $|Y|^2$ is the squared magnitude of admittance before TTX at 30-mV depolarization (2.8×10^{-7} S^2 at 1 kHz). Thus the power spectral density at 1 kHz in TTX underestimates the actual background noise by 31%. As seen in Fig. 4, alteration of $|Y|$ affects S_{I_b}, which in turn affects the correction of $S_{I_{Na}}$ at frequencies above 800 Hz. Hence the underestimate of S_{I_b}, by use of the TTX spectrum as background noise, produces significant distortion of spectral shape as well as errors in intensity, which can be avoided by use of the alternative procedure.

Estimation of Linear Parameters from Na Admittance Data

The frequency-domain manifestation of time- and voltage-dependent Na conduction has been described and discussed qualitatively in a previous report (Fishman et al., 1979). In the present experiments, a quantitative linear analysis is required. Because of the remarkably good account of previous admittance data provided by the linearized Hodgkin-Huxley (HH) equations, the expression for the admittance derived from these equations was used as the basis for curve fitting the admittance data. In particular, the admittance of the circuit of Fig. 7 was used to fit the complex admittance data, as described in the Methods section, to extract each of eight parameters in the circuit model.

Element C_M^* is a constant-phase-angle capacitance, used by Cole and Cole (1941) to take into account dielectric loss. The admittance of C_M^* is then

$$Y_{C_M^*} = (j\omega)^\alpha C_M^* = C_M^* \omega^\alpha \left(\cos\frac{\alpha\pi}{2} + j \sin\frac{\alpha\pi}{2}\right), \qquad (1)$$

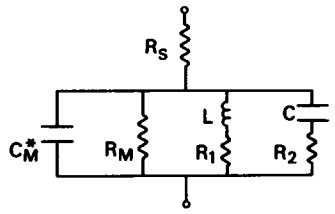

FIGURE 7 Linear circuit model used to fit admittance data. The symbol C_M^* refers to the constant-phase-angle capacitance described by Cole and Cole (1941) to account for dielectric loss; see Eq. 1. The other circuit elements conform to the linearized HH model, as described in the text.

where α is the ratio of the actual asymptotic phase angle of C_M^* to the ideal value of 90°, and ω is the angular frequency $2\pi f$. R_M is the frequency independent part of membrane resistance. The R_1-L branch models the first-order frequency domain behavior of Na-conduction inactivation and the R_2-C branch the first-order behavior of Na-conduction activation (Cole, 1972, p. 299). A series resistance, R_S, is included to take into account the access paths to the membrane surfaces from the potential sensing electrodes.

Generally, the circuit model of Fig. 7 was found to produce the best (in the chi-square sense) admittance fits of all the measured data. Without exception the use of an ideal capacitance for C_M^* yielded higher chi-square values for fits of data and was rejected in favor of the constant-phase-angle formulation, despite the lack of a physical explanation for the phenomenon that produces this effect. Fernandez et al. (1982) have also measured the complex admittance of squid axon in approximately the same frequency range, but during suppressed ion conduction. Their data, after correction for a lumped series resistance, could be fitted without a constant-phase-angle assumption. As pointed out by them, the correction for series resistance is essential for a determination of membrane capacitance. Such corrections are complicated by the fact that the series resistance is actually a complex impedance (Leuchtag et al., 1982). This may account for the better fits that we obtained using a constant-phase-angle capacitor with the series resistance in our model (Fig. 7). In any event, the major findings in this work are not dependent upon the constant-phase-angle assumption (see Discussion). Also reduction in the number of circuit elements in Fig. 7 yielded significantly inferior fits of the data.

Fig. 8 *a* shows a typical set of complex admittance data plotted as log magnitude and phase angle vs. log frequency. These data were acquired in an 80 ms interval, 5 s after single step clamps of the values indicated. These admittance determinations showed no significant variations when evaluated at other times (0.3 to 24 s) after a step clamp. Thus they are steady-state admittances. The solid curves are the best fits to the sets of 400 complex data points of the admittance of the circuit in Fig. 7. At holding potential (0-mV displacement) the phase function, at low frequencies, is close to zero and increases monotonically to

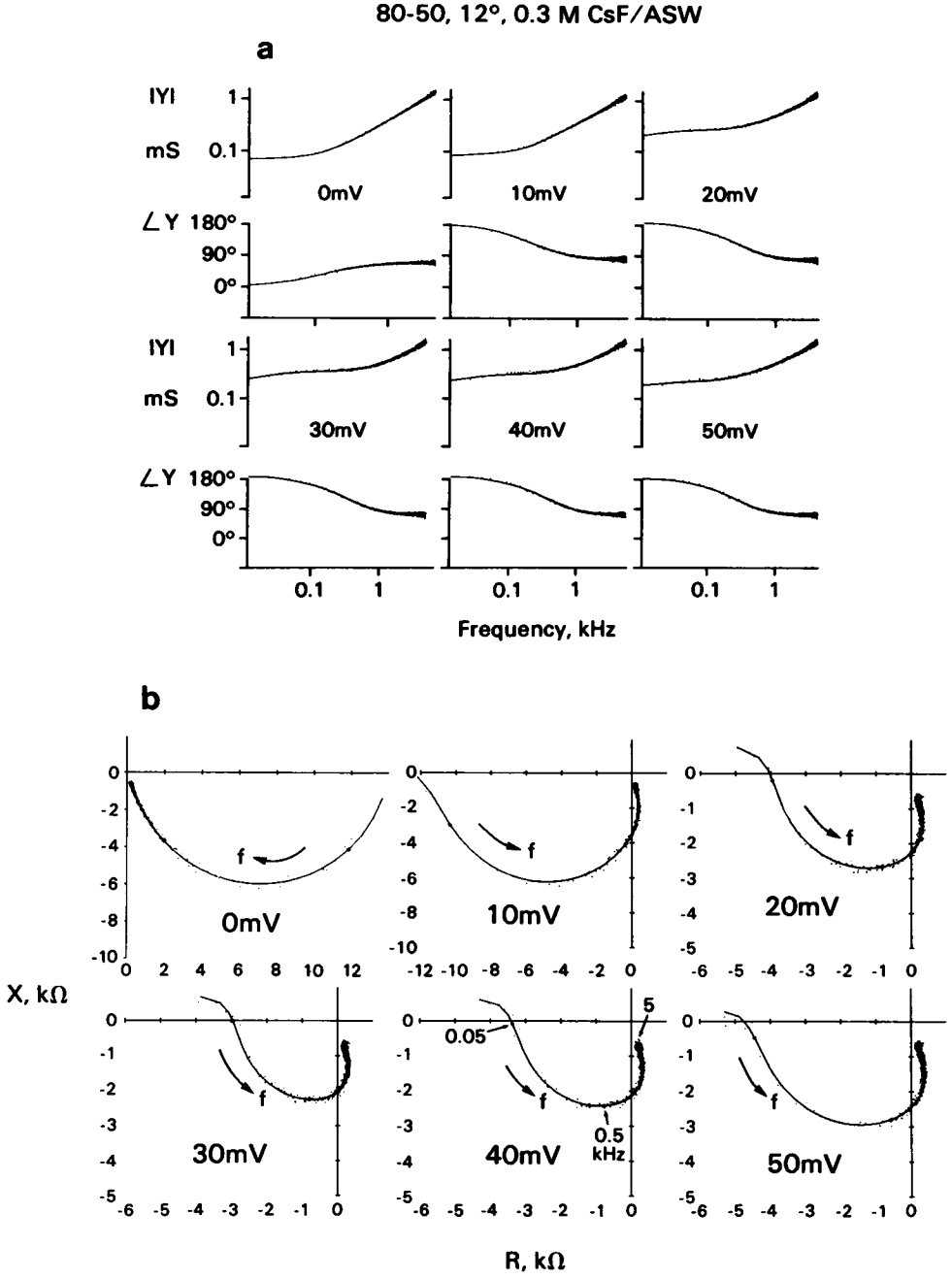

FIGURE 8 (*a*) Admittance magnitude and phase of squid axon with potassium conduction suppressed. Each complex admittance was determined by an FFT of the current response to a synchronized, Fourier-synthesized pseudorandom signal (FSPS) (≈1 mV peak-to-peak) superposed as a continuous, repetitive perturbation on a single-step voltage clamp. The portion of the response that carries the admittance information was obtained from a time sample record, of a single FSPS period (80 ms in length), acquired 5 s after a step clamp. The admittance for the indicated step voltages from an estimated holding potential of −60 mV showed no significant variations when they were evaluated at other times (0.3 to 24 s) after a step clamp. Thus these measurements were made during a steady state. The points represent data and the lines are best fits to the data based on the circuit in Fig. 7, with parameters given in Table I. Note that the phase at 0 mV rises smoothly from 0°, while at depolarizations the phases decrease monotonically from ~180°, indicative of a negative conductance. Axon area ~0.08 cm^2. Series resistance compensation for 3.6 Ω · cm^2. (*b*) Complex-plane plots of squid-axon impedance, obtained from the same data and fits as *a*. *Abscissa:* resistance in kilohms; *ordinate:* reactance in kilohms. Again note the difference between the 0 mV record, for which the resistance (real part of complex impedance) is positive throughout, and the others, which have negative resistance in the low-frequency range. Circles (●) mark the 0.05, 0.5, and 5 kHz points; the initial points are at 0.0125 kHz.

~76° at 5 kHz. However, for each of the subsequent depolarizations (10, 20, 30, 40, 50 mV) from the holding potential (~−60 mV) the phase is 180° at low frequency and decreases to ~80° at 5 kHz. The 180° phase at low frequency is indicative of a steady-state negative conductance. Confirmation of the interpretation of the 180° phase angle at depolarized potentials is shown in Fig. 8 *b* in which the same complex data are plotted as impedance loci in the complex plane. For depolarized potentials the real part of the impedance is negative at frequencies below 1 kHz. This condition was observed and discussed in previous measurements (Fishman et al., 1979), where it was demonstrated that these admittance data reflect Na conduction as well as leakage conduction and capacitance.

Table I contains the model parameter estimates from curve fits of admittance data from three different axons. Note that the values for R_M for depolarized potentials are all negative, which corroborates the interpretation of a 180° phase angle in the admittance at low frequency. In obtaining the parameter estimates in Table I, all eight parameters were free to be changed by the curve-fitting program; nevertheless, the best fits yielded values for C_M^* and α that were relatively independent of potential. While the value of C_M^* obtained for any given axon was constant, it varied from axon to axon due to variations in axon diameter. However, α was found to be ~0.9, independent of axon geometry. An α of 0.9, corresponding to a constant phase angle of 81°, is in the range found previously by Cole and Curtis (1938) in transverse measurements of impedance, done with electrodes entirely outside the axon. A series resistance element was required for model fits of admittance data despite compensation for the value of R_S that was determined from high-frequency impedance measurements (see the Methods section: Series Resistance Compensation). This discrepancy is probably due to the significant contribution to the admittance by membrane ion conduction in the 5-kHz frequency range. Thus estimates of R_S from model fits of low frequency admittance data are less accurate than those determined at higher frequencies. Another possibility, for which there is some evidence (Leuchtag et al., 1982), is that the access to the membrane is a complex impedance that cannot be modeled as a lumped series resistance at intermediate frequencies.

The parameters of prime interest in Table I are those for the R_1-L and R_2-C branches of Fig. 7. These are the elements that account for the temporal variation of Na conductance and provide the linear macroscopic estimates of the kinetics. Two natural frequencies, which are to be compared with the corner frequency estimates from spectral analysis of Na-current noise, are computed as a low-frequency component, $f_1 = L/R_1$, and a higher-frequency component $f_2 = R_2C$. These may be associated with the linearized Hodgkin-Huxley formulation by the relations (Cole, 1972), $f_1 = (2\pi\tau_h)^{-1}$ and $f_2 = (2\pi\tau_m)^{-1}$, where τ_h and τ_m are the relaxation times of Na inactivation and activation processes.

TABLE I
LINEAR MODEL PARAMETER ESTIMATES FROM CURVE FITS OF ADMITTANCE DATA

V	C_M^*	α	R_M	R_S	R_1	L	C	R_2	f_1	f_2	χ^2
(*mV*)	(*μF*)		(*kΩ*)	(Ω)	(*kΩ*)	(*H*)	(*nF*)	(*kΩ*)	(*Hz*)	(*Hz*)	
Experiment no. 80–43, 13°, area ≈ 0.1 cm²											
−10	0.20	0.89	18.5	22	—	—	20	19.5	—	410	0.007
10	0.21	0.90	−24.4	73	2.7×10^4	6.4×10^4	106	10.0	73	151	0.013
15	0.29	0.87	−6.3	53	24.6	148	200	6.7	26	120	0.029
20	0.21	0.89	−1.3	61	2.2	24	296	1.1	14	502	0.009
30	0.26	0.87	−1.3	51	1.7	7.9	310	0.9	33	556	0.011
40	0.26	0.87	−1.9	55	2.2	6.8	290	1.0	52	544	0.008
50	0.21	0.89	−2.3	64	2.7	7.5	250	1.1	57	573	0.012
Experiment no. 80–48, 12.5°, area ≈ 0.1 cm²											
−10	0.17	0.91	14.0	39	—	—	—	—	—	—	0.008
0	0.17	0.91	15.0	28	—	—	32	6.1	—	805	0.005
10	0.17	0.90	−6.7	19	6.6	1.3×10^5	281	5.5	83	102	0.006
15	0.17	0.91	−11.2	50	23.4	50	106	9.4	73	161	0.008
20	0.17	0.91	−6.3	40	50.6	400	76	5.7	20	364	0.007
30	0.17	0.91	−1.8	43	3.9	29	227	1.3	21	550	0.006
40	0.18	0.91	−1.6	45	4.1	30	254	1.1	21	553	0.008
50	0.18	0.91	−1.7	53	5.8	41	267	1.2	22	507	0.008
Experiment no. 80–50, 12°, area ≈ 0.08 cm²											
−20	0.13	0.92	17.3	64	—	—	9	17.3	—	993	0.004
0	0.13	0.91	13.9	76	—	—	7	25.5	—	868	0.003
10	0.13	0.90	−10.4	60	58.0	386	31	6.8	24	754	0.005
20	0.12	0.91	−3.7	63	10.2	73	85	3.0	22	622	0.004
30	0.12	0.91	−2.7	65	6.8	41	124	2.3	26	553	0.004
40	0.13	0.90	−3.1	68	8.4	50	108	2.6	27	572	0.004
50	0.13	0.90	−4.1	70	15.7	84	87	3.1	30	591	0.005

Na-Noise Spectra and Curve Fits

The Na-current fluctuations were acquired and their spectra were computed immediately after an admittance run in each axon. As described earlier, the fluctuations were stationary in the interval 0.3 ms to 12 s after step changes of membrane potential. Thus, an average power spectrum of 64 individual spectra in the frequency range 12.5 Hz–5 kHz was produced by applying a step clamp of the same value for which admittance data were obtained, and continuously analyzing the fluctuations for 12 s. The acquired averaged spectra were automatically corrected for the passband characteristics of the signal processing instrumentation and were corrected for background current noise at each potential before curve fitting, as described in the Methods section. The results of one particular experiment on the same axon from which the admittance data of Fig. 8 were obtained is shown in Fig. 9. The solid lines are curve fits of the 400-point spectral data at each potential to a spectrum calculated as the sum of two Lorentzian functions. That is, each spectrum was fitted with the function

$$S_{I_{Na}} = \frac{A_1}{1 + (f/\nu_1)^2} + \frac{A_2}{1 + (f/\nu_2)^2}, \quad (2)$$

and values for A_1, ν_1, A_2, and ν_2 were obtained that minimized the chi-square value for the model with respect to the data. Because of the limited spectral data (2 decades in frequency), it was not possible to obtain unique fits of the data with more than two Lorentzian functions, despite the expectation of multiple components from the HH formulation. Nevertheless, this is not arbitrary because the multiple Lorentzian terms in the HH power spectrum are related in frequency and cluster to give essentially a double bump spectrum with asymptotic behavior that is indistinguishable from a two-Lorentzian spectrum. Furthermore, our rationale in these experiments was to compare the spontaneous noise with a linear perturbation response to determine if they gave the same result. The HH model for Na when linearized does contain only two Lorentzian terms in the power spectrum so that this analysis is a rigorous test of the question: does the linear response predict the noise?

Near holding potentials, 0 and 10 mV, spectral data from some axons could be fitted with a $1/f$ term added to the above function, but these fits were not better than the ones using only two Lorentzians and therefore were not used in further data analyses. In contrast to the form of the spectra of K current noise, which has a strong $1/f$ component, and the single Lorentzian fit of spectra of Na current noise obtained previously in squid axon with an axial-wire technique (Conti et al., 1975), the Na current-noise spectra under the condition of internal Cs perfusion, of which Fig. 9 is typical, exhibit two clear humps and were best fitted without an $1/f$ component.

Table II contains a summary of the double Lorentzian-model curve fits of power spectra in the same three experiments for which admittance curve fits were obtained (Table I). Generally, the intensities A_1 and A_2 of the Lorentzian components increase monotonically as the axon is depolarized over a 50-mV range from the holding potential. The variation of corner frequencies, ν_1 and ν_2, with potential, on the other hand, is not monotonic.

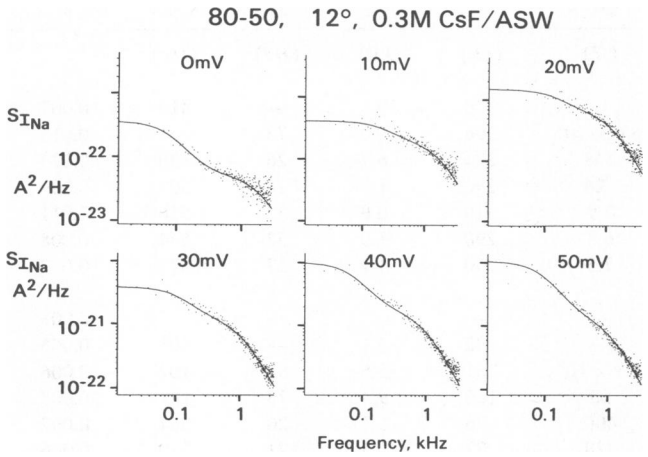

FIGURE 9 Power spectra of spontaneous fluctuations in Na current of the same squid axon from which the data in Fig. 8 were obtained, and under the same conditions. The current noise density was recorded in the frequency range 12.5–5,000 Hz during the interval 0.3–12 s after the step voltage changes indicated from an estimated holding potential of −60 mV. The stationarity of the current noise during this interval is shown in Fig. 5. Spectral corrections as illustrated in Fig. 4 have been applied to the data. A double Lorentzian function, Eq. 2, was fitted to the data, with parameters given in Table II. Series resistance compensation for 3.6 Ω · cm².

Na-Channel Conductance vs. Potential

With the assumption of the ion-channel hypothesis, in which all channels are taken to be identical, independent, and to have a single open conducting state, the Na-channel conductance, γ_{Na}, may be calculated from the following relation (Neher and Stevens, 1977)

$$\gamma_{Na} = \frac{\sigma^2_{I_{Na}}}{\langle g_{Na} \rangle (V - V_r)^2}, \quad (3)$$

where V is the step voltage from holding, V_r is the step voltage that gives zero current after leakage removal, $\sigma^2_{I_{Na}}$ is the variance of Na-current fluctuations, and $\langle g_{Na} \rangle$ is the mean Na conductance. The use of Eq. 3 assumes that the probability of channels opening in the explored potential range is much <1. This assumption is reasonable under the conditions of measurement since the mean Na current during the steady-state noise measurement interval did not exceed 10% of the peak inward current during the transient phase. Thus most of the channels remained closed during the noise measurements. This assumption is also consistent with the values obtained for $\langle g_{Na} \rangle$ in Table II.

Estimates of $\langle g_{Na} \rangle$ were obtained in two ways. First, from curve fits of $Y(j\omega)$, $\langle g_{Na} \rangle$ is available from the

TABLE II

TWO LORENTZIAN MODEL: PARAMETER ESTIMATES FROM CURVE FITS OF NOISE POWER SPECTRA

V	A_1	ν_1	A_2	ν_2	χ^2	$\langle g_{Na} \rangle$	σ_1	σ_2^2	γ_{Na}
(mV)	$(10^{-22}A^2/Hz)$	(Hz)	$(10^{-22}A^2/Hz)$	(Hz)		(mS)	$(10^{-20}A^2)$	$(10^{-20}A^2)$	(pS)
Experiment no. 80–43, 13°, V_r = 155 mV									
5	6.2	82	0.6	1,300	0.001	0.03	8.0	13.1	0.3
10	24.1	73	3.2	1,209	0.002	0.10	29.6	60.6	0.4
15	28.4	78	14.7	873	0.003	0.17	34.8	201.6	0.7
20	149.5	100	25.9	884	0.001	0.37	234.4	359.6	0.9
30	158.0	194	16.1	884	0.0004	0.24	480.2	223.6	1.9
40	208.0	105	21.5	863	0.0004	0.13	342.1	291.4	3.8
50	166.0	127	16.9	1,115	0.0005	0.12	330.6	296.0	4.8
Experiment no. 80–48, 12.5°, V_r = 135 mV									
10	3.2	108	0.7	243	0.016	0.07	5.4	2.7	0.07
15	5.8	121	1.3	371	0.002	0.12	11.1	7.8	0.11
20	12.7	142	1.2	486	0.002	0.21	28.4	9.2	0.13
30	44.6	92	6.2	1,212	0.002	0.36	64.1	118.1	0.45
40	59.5	90	16.1	1,075	0.003	0.45	84.1	271.7	0.87
50	96.8	70	25.0	903	0.0003	0.50	106.7	354.5	1.3
Experiment no. 80–50, 12°, V_r = 145									
0	3.1	85	0.51	1,999	0.004	0.04	4.1	16.0	0.2
10	2.3	247	1.9	1,819	0.007	0.14	8.9	53.1	0.3
20	8.7	175	6.3	1,317	0.001	0.23	23.9	130.3	0.4
30	27.3	128	11.6	1,085	0.002	0.28	54.9	197.7	0.7
40	85.6	75	15.9	954	0.0003	0.26	100.4	238.3	1.2
50	95.7	99	12.2	1,119	0.0002	0.24	149.1	214.4	2.7

estimates of R_M in the model of Fig. 7. The membrane leakage resistance was taken as the value for R_M obtained from curve fits of admittance data at potentials sufficiently hyperpolarized (usually 20 mV) from holding to yield an admittance that could be fitted with only the R_M and C_M^* branches in the membrane circuit model. Because the R_1-L and R_2-C branches model the time- and voltage-dependent Na conductance in the frequency domain, the Na conductance is insignificant whenever these branches can be excluded in a fit of the data; under these conditions R_M may be taken as an estimate of leakage. The leakage resistance, assumed to be linear, was then removed from the value of R_M obtained in curve fits of $Y(j\omega)$ data at all other potentials (rest and depolarizations) for which the R_1-L and R-C branches were required for fits. The reciprocal of the resulting resistance at each potential was taken as $\langle g_{Na} \rangle$ and is shown for the representative experiment in the uppermost curve of Fig. 10.

As a check of the above procedure for determination of $\langle g_{Na} \rangle$, estimates of g_M were obtained by curve fits of $Y(j\omega)$ with the linearized model before and after elimination of g_{Na} with TTX (1 μM). The estimated value of g_M after TTX was taken as leakage and subtracted from the value before TTX for pairs of $Y(j\omega)$ data at the same membrane potential. One set of estimates of $\langle g_{Na} \rangle$, determined in this manner, are shown as open circles in the upper most portion of Fig. 10. These data were obtained in a different axon and scaled (by the factor 1.4) to the area of axon 80–50. The TTX subtracted data show reasonable agreement with the previous procedure and confirm the functional dependence of $\langle g_{Na} \rangle$ on potential. In addition, $\langle g_{Na} \rangle$ was calculated from the relation $g_{Na} = \bar{g}_{Na} m_\infty^3 h_\infty$, where $\bar{g}_{Na}$, m_∞, and h_∞ are the HH parameters with the HH values assumed and scaled to a membrane area of 0.08 cm^2. Comparison of the curve labeled $\bar{g}_{Na}\, m_\infty^3 h_\infty$ in Fig. 10 with the experimental determinations of $\langle g_{Na} \rangle$ show that the potential dependence of $\langle g_{Na} \rangle$ is as expected from the HH formulation, but the magnitudes of the experimentally determined values of $\langle g_{Na} \rangle$ are much larger. The larger magnitudes arise from the internal perfusion with Cs, which is known to produce substantial steady-state Na current due to partial removal of Na inactivation (Chandler and Meves, 1965, 1970).

The variance of Na-current fluctuations, $\sigma^2_{I_{Na}}$, at each potential was obtained from the double Lorentzian fits of $S_{I_{Na}}$ (Fig. 9). The variance is given by (Neher and Stevens, 1977)

$$\sigma^2_{I_{Na}} = \frac{\pi}{2}(A_1\nu_1 + A_2\nu_2), \tag{4}$$

using estimates for A_1, ν_1, A_2, and ν_2 (Table II). The middle curve in Fig. 10 shows $\sigma^2_{I_{Na}}$, calculated from Eq. 4, as a function of potential for the typical experiment.

The data shown in Fig. 10 for γ_{Na} vs. potential were calculated in this way with V_r = 145 mV. Clearly γ_{Na} is voltage dependent, ranging from 0.2 to 1.7 pS for depolarizations of 0 to 50 mV from an absolute holding potential of ~ -60 mV. The data from two other axons (Table II) show the same increasing trend in γ_{Na} with depolarized voltage and values ranging from 0.1 to 4.8 pS over the same potential range. Furthermore, if the probability of open

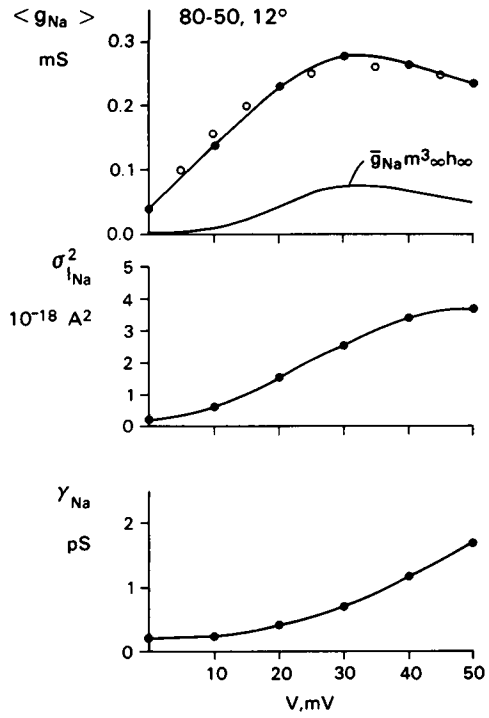

FIGURE 10 Calculation of "single, Na channel conductance" and its voltage dependence based on the ion channel hypothesis. *Top:* Mean Na conductance, $\langle g_{Na} \rangle$, vs. step potential from holding. Open circles are corroborative determinations of $\langle g_{Na} \rangle$ from curve fits of $Y(j\omega)$ data after removal of leakage, estimated from curve fits of $Y(j\omega)$ data in TTX at the corresponding potentials. Open circle data (O) were obtained on a different axon and scaled (1.4 ×) to that of the area (0.08 cm²) of axon 80–50. Curve labeled $\bar{g}_{Na}m^3_\infty h_\infty$ is the HH prediction of $\langle g_{Na} \rangle$ assuming HH parameter values and scaled to an area of 0.08 cm². See text for further details. *Middle:* Sodium-current variance, $\sigma^2_{I_{Na}}$, obtained from double Lorentzian fits (Eq. 4, Fig. 9, and Table II) vs. step potential. *Bottom:* Single-channel conductance, γ_{Na}, calculated from Eq. 3 using the above variance, conductance values, and a reversal potential of 145 mV from holding. γ_{Na} is clearly voltage dependent. The potential dependence of γ_{Na} for this axon and two additional ones are given in Table II.

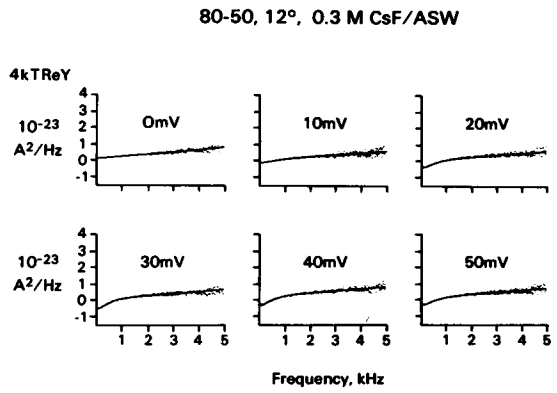

FIGURE 11 Conduction noise predicted by the Nyquist relation, Eq. 5, for the axon of Figs. 8 and 9. *Abscissa:* Linear frequency axis; *ordinate:* linear scale of the quantity $4kT\mathrm{Re}Y$, the theoretically predicted equilibrium conduction noise. The ReY used in these plots was obtained from the $Y(j\omega)$ data in Fig. 8 *a*. Comparison with Fig. 9 (which has logarithmic axes) shows that the conduction noise given by the Nyquist relation is considerably less than the actual noise observed. The shape of the observed noise spectrum is also entirely different. Both of these results indicate that Na current noise reflects a nonequilibrium process. The fluctuation-dissipation theorem (Kubo, 1957) does not apply.

channels is not <1, as was assumed in these calculations, the size of the increase of γ_{Na} with depolarization shown in Fig. 10 would be underestimated.

DISCUSSION

Na-Current Fluctuations Exceed the Nyquist Prediction

In these experiments, both the power spectrum of Na-current fluctuations, $S_{I_{Na}}$, and the complex admittance, $Y(j\omega)$, of a predominantly Na-conducting membrane were measured under the same conditions of voltage, internal and external solution ionic composition and temperature, and in the same axons. Thus the intensity and form of current-noise power spectra can be compared quantitatively with the expectations from the Nyquist relation, given by

$$S_I(f) = 4kT\mathrm{Re}Y(j\omega), \quad (5)$$

where k is Boltzmann's constant, T is absolute temperature, and Re$Y(j\omega)$ is the real part of the complex admittance. Fig. 11 shows power spectra calculated from the real part of the measured complex admittance data in Fig. 8 and the Nyquist relation. Although spectral components in Fig. 11 are plotted as a linear rather than a logarithmic function of frequency, clearly a comparison of the Nyquist prediction with the measured $S_{I_{Na}}$ in Fig. 9 at each corresponding potential shows that the spectral intensities of Na-current fluctuations are substantially in excess of the Nyquist prediction, and that they do not agree in form. A similar result for the K-current process in squid axon has been reported previously (Conti et al., 1975).

The inapplicability of the Nyquist theorem means that the fluctuation-dissipation theorem (Kubo, 1957) is also not valid for the Na system. This result is not surprising in view of the fact that the macroscopic Na-conduction process is both nonlinear and yields a steady-state negative conductance, as shown in Fig. 8 and discussed earlier, whereas the Nyquist relation is derived assuming a linear system and thermal equilibrium. Whether or not it is possible to infer anything further about the microscopic Na-conduction system from these data depends upon recent developments of thermal-noise concepts for nonlinear systems (Gupta, 1982).

In the channel model of membrane conduction it is assumed that conduction can be described by independent and distinct processes, namely, gating, conductance, and driving force. It is further assumed in this hypothesis that nonequilibrium conditions can be attributed exclusively to the driving force while gating and conductance are equilibrium processes that are independent of ion concentration gradients. Although our measurements show that Na

conduction is a nonequilibrium process, this result is consistent with the above hypothesis. Frehland (1980, 1982) and Frehland and Faulhaber (1980) have shown that an ionic gradient in conjunction with an equilibrium gating process can generate excess noise.

Na-Channel Conductance

With respect to previous Na-current fluctuation measurements in the squid axon, Conti et al. (1975) obtained a γ_{Na} of 4 pS for changes in membrane potential under axial-clamp conditions of up to 20 mV from holding potential and in unperfused axons. In their experiments, a Na-current fluctuation spectrum was determined either as the spectrum of fluctuations after injection of tetraethylammonium (TEA) ions or from the difference between spectra before and after the external application of TTX. The use of TEA to suppress K-current fluctuations in squid axon was shown to be an ambiguous procedure, because TEA induces substantial K-conduction noise even though the mean K current is reduced significantly (Fishman et al., 1975*b*, 1977; Moore et al., 1979). The use of spectra after TTX to remove background noise can produce significant errors in Na-noise spectral estimates due to alteration of the membrane admittance after TTX, which in turn results in an underestimation of background noise as described in the Results section. The Conti et al. (1975) study indicated that γ_{Na} is not voltage dependent as opposed to our finding that it is. The factors mentioned above may account for the differences in the two studies.

In our previous measurements of Na-current fluctuations in squid axon, using an external patch-clamp technique (Fishman et al., 1977), we reported that the spectral form appeared to be more complicated than a single Lorentzian function and that γ_{Na} was voltage dependent. The results here, which were obtained by axial-electrode technique on much larger membrane areas, confirm these measurements.

The finding that γ_{Na} is voltage dependent is also at variance with interpretations of Na-current noise measurements in node of Ranvier preparations (Conti et al., 1976, 1980; Sigworth, 1977). In the second study, γ_{Na} was found to increase with increasing depolarizations; however, this increase was attributed to improper corrections for insufficient bandwidth in the clamp and nonstationary conditions. Again, improper correction for background noise in the node experiments may have been a factor in the interpretations. Background noise was assumed to be eliminated by subtracting power spectra and σ_I^2 after TTX from those data obtained before TTX. As discussed earlier, this procedure may not be valid in preparations in which the voltage- and time-dependent Na conductance contributes significantly to membrane admittance, because the background current-noise changes with variations in (ionic) admittance. There is no published report on the effect of TTX on the complex admittance of the nodal membrane. Nevertheless, in theoretical calculations the nodal impedance shows a substantial dependence on the presence of an operative Na conductance (Clapham and DeFelice, 1976). Consequently, there is some uncertainty in estimates of $\sigma^2_{I_{Na}}$ obtained from power spectra in previous nodal Na current-noise measurements.

Nonstationary noise analyses, during Na-current transients, have also yielded estimates of γ_{Na} of 8 pS in the frog-node preparation (Sigworth, 1977). The single-channel conductance remained unchanged after substantial changes in membrane peak Na conductance. These and other results were consistent with a simple open-closed channel. Nevertheless, unambiguous information can be obtained from nonstationary fluctuations only for the simplest kind of process. Noise data acquired during transients do not permit spectral determinations. Without spectral data, it is difficult to assess background and other noise contributions to the variance of fluctuations.

Because our finding that γ_{Na} is voltage dependent is not in agreement with the other studies mentioned above, we examine the possible sources of error. From Eq. 3, our determinations of γ_{Na} depend on estimates of $\langle g_{Na} \rangle$, V_r, and $\sigma^2_{I_{Na}}$. It is unlikely that the voltage dependence of $\langle g_{Na} \rangle$ is a significant source of error because the shape of the curve in Fig. 10 was corroborated independently by determinations after TTX and is in agreement with the shape expected from the HH formulation. Errors in estimates of V_r are also not likely to account for the voltage dependence of γ_{Na} because, at the maximum depolarization of 50 mV from holding, the influence of the term $(V\text{-}V_r)$, where V_r ranged from 135 to 155 mV from holding, is small. These considerations lead to the conclusion that the voltage dependence of γ_{Na} is directly attributable to our estimates of $\sigma^2_{I_{Na}}$, which come from the model fits of corrected spectra such as those shown in Fig. 9. Although corrections for background noise in spectral data are necessary with the present techniques, the measurement and use of membrane admittance at the same potentials and in the same axons appears to provide the best available method of minimizing spectral distortion.

The finding that γ_{Na} is voltage dependent requires reexamination of the interpretation of Eq. 3. Chen (1976) has shown that whenever the right-hand side of Eq. 3 is voltage dependent, the channel must conduct in more than one open state. A multiconductance channel could be produced by a voltage-dependent open-channel conductance or by the "gating" process. There is some evidence in support of a voltage-dependent sodium-channel conductance. Yamamoto et al. (1982) reported a calcium-dependent nonlinear single-channel current-voltage relation in neuroblastoma cells and Taylor et al. (1976) obtained a calcium-dependent nonlinear instantaneous sodium current-voltage relation in squid axon. Furthermore, because the current fluctuations were measured from a large population of channels, the possibility of nonidentical channels cannot be excluded.

Linear and Fluctuation Analyses Yield Different Kinetic Parameters for Na Conduction

A linear analysis of Na conduction was done by fitting complex admittance data obtained during step clamps with the admittance of a linear circuit model, thereby yielding the best (least-squares fit) estimates of the model parameters. The use of a circuit model does not compromise the determination of the kinetic parameters because the circuit model is a direct realization of an HH type analytical expression for the membrane admittance, namely,

$$Y_M(j\omega) = j\omega C^* + g + \frac{g_1}{1 + j\omega\tau_1} + \frac{g_2}{1 + j\omega\tau_2}, \qquad (6)$$

where the relaxation times, τ_1 and τ_2, are identical to $(2\pi f_1)^{-1}$ and $(2\pi f_2)^{-1}$, respectively, and the g's are voltage-dependent conductances. Although the particular circuit realization (Fig. 7) of the admittance expression is not unique, the estimates of the natural frequencies, f_1 and f_2, are. The validity of this statement is based on the fact that all circuit realizations of the admittance expression must yield the same two natural frequencies. Furthermore, the quality of the fits (Fig. 8 *a*, *b*) indicate that the assumed model gives an adequate description. Significantly poorer fits (larger chi-squared) were obtained when a reduction in the number of circuit elements was attempted. A two-time-constant model thus appears to be the simplest one that can account for the data.

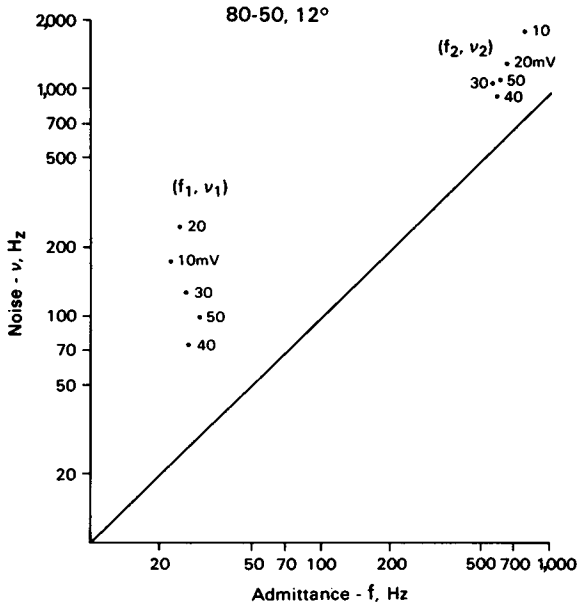

FIGURE 12 Relationship between the lower (f_1) and upper (f_2) natural frequencies obtained from admittance, and lower (ν_1) and upper (ν_2) corner frequencies from noise measurements in the same axon. The *abscissa* indicates the frequency obtained from the admittance data for a given potential, and the *ordinate*, the corresponding frequency from the noise data. Note the greater voltage dependence of the characteristic noise frequencies than those of the characteristic admittance frequencies. The squid axon is the same as in the previous three figures. Table III contains this comparison for this and two other axons.

Fig. 12 shows a plot of the corner frequencies obtained from fits of $S_{I_{Na}}$ (Fig. 9) with the sum of two Lorentzian functions vs. the two natural frequencies determined by linear analysis of the admittance at the indicated depolarized potentials from holding. The solid line through the origin is the line on which the data points should fall if the curve fits of data at the same potential yielded the same values. The estimates of ν_1 and ν_2 from noise data were always significantly higher (by factors of 1.7 to 10.3 times in this case) than those of f_1 and f_2 obtained from admittance data. Table III contains this comparison for three different axons. The additional axon data presented in the table reinforce the above result. Clearly this disagreement in the determination of the kinetic parameters of the Na system between fluctuation and linear analysis indicates that the kinetics of the microscopic process, as reflected in the fluctuations, are not adequately determined from an admittance analysis and therefore reflect nonlinearity. This result was not dependent on the assumption of a constant-phase-angle capacitance in the linear model fits of $Y(j\omega)$ data. Fits without the constant phase angle were poorer, but still gave natural frequencies that were significantly lower than the corresponding corner frequencies in noise spectral analyses.

Analysis of the response to small perturbations provides a linear, macroscopic, phenomenological description of a system about an operating point. However, van Kampen (1969) has shown that macroscopic linearity is not the same as linearity of the microscopic equations of motion of

TABLE III
COMPARISON OF CHARACTERISTIC FREQUENCIES OBTAINED FROM NOISE (ν) VS. ADMITTANCE (f) ANALYSIS

V	ν_1	f_1	ν_1/f_1	ν_2	f_2	ν_2/f_2
(*mV*)	(*Hz*)	(*Hz*)		(*Hz*)	(*Hz*)	
Experiment no. 80–43, 13°						
10	73	73	1.0	1,209	151	8.0
15	78	26	3.0	873	120	7.3
20	100	14	7.1	884	502	1.8
30	194	33	5.9	884	556	1.6
40	105	52	2.0	863	544	1.6
50	127	57	2.2	1,115	573	1.9
Experiment no. 80–48, 12.5°						
10	108	83	1.3	243	102	2.4
15	121	73	1.7	371	161	2.3
20	143	20	7.2	486	364	1.3
30	92	21	4.4	1,212	550	2.2
40	90	21	4.3	1,075	553	1.9
50	70	22	3.1	903	507	1.8
Experiment no. 80–50, 12°						
10	247	24	10.3	1,819	754	2.4
20	175	22	8.0	1,317	622	2.1
30	128	26	4.9	1,085	553	2.0
40	75	27	2.8	954	572	1.7
50	99	30	3.3	1,119	591	1.9

all particles in a system. Thus in the case of a nonlinear microscopic membrane process, the fluctuation spectrum is not necessarily determined by the macroscopic linear behavior, and hence the discrepancy between the kinetic parameters obtained from the two types of measurements on the Na system may be expected to arise on theoretical grounds. These results reinforce the notion that a physical theory of conduction must be capable of explaining the fluctuation data, because only the fluctuations reflect the microscopic motions of all the charged particles in the system.

We thank Dr. Jorge Sanchez for assistance in the experiments during his Grass Fellowship. Dr. Tatsuo Iwazumi designed the low-noise primary stage to the voltage clamp and Mr. Michael Fason constructed it. Ms. Sarah Adams typed the manuscript version of this paper.

This work was done at the Marine Biological Laboratory, Woods Hole, MA and was supported in part by a U. S. Public Health Service grant NS11764.

Received for publication 4 January 1983 and in final form 26 April 1983.

REFERENCES

Bevington, P. R. 1969. Data Reduction and Error Analysis for the Physical Sciences. McGraw-Hill, Inc., New York.

Chandler, W. K., and H. Meves. 1965. Voltage clamp experiments on internally perfused giant axons. *J. Physiol. (Lond.).* 180:788–820.

Chandler, W. K., and H. Meves. 1970. Sodium and potassium currents in squid axons perfused with fluoride solutions. *J. Physiol. (Lond.).* 211:623–652.

Chen, Y. 1976. Differentiation of channel models by noise analysis. *Biophys. J.* 16:965–971.

Clapham, D. E. and L. J. DeFelice. 1976. The theoretical small signal impedance of the frog node, *Rana pipiens. Pfluegers Arch. Eur. J. Physiol.* 366:273–276.

Cole, K. S. 1972. Membrane, Ions and Impulses. University of California Press, Berkeley.

Cole, K. S., and R. H. Cole. 1941. Dispersion and absorption in dielectrics. I. Alternating current characteristics. *J. Chem. Phys.* 9:341–351.

Cole, K. S., and H. J. Curtis. 1938. Transverse electric impedance of the squid giant axon. *J. Gen. Physiol.* 21:757–765.

Cole, K. S., and U. Kishimoto. 1962. Platinized silver chloride electrode. *Science (Wash, DC).* 136:381–382.

Conti, F., L. J. DeFelice, and E. Wanke. 1975. Potassium and sodium ion current noise in the membrane of the squid giant axon. *J. Physiol. (Lond.).* 248:45–82.

Conti, F., B. Hille, B. Neumcke, W. Nonner, and R. Stämpfli. 1976. Measurement of the conductance of the sodium channel from current fluctuations at the node of Ranvier. *J. Physiol. (Lond.).* 262:699–727.

Conti, F., B. Neumcke, W. Nonner, and R. Stämpfli. 1980. Conductance fluctuations from the inactivation process of sodium channels in myelinated nerve fibres. *J. Physiol. (Lond.).* 308:217–239.

DeFelice, L. J., E. Wanke, and F. Conti. 1975. Potassium and sodium current noise from squid axon membranes. *Fed. Proc.* 34:1338–1342.

Fernandez, J. M., F. Benzanilla, and R. E. Taylor. 1982. Distribution and kinetics of membrane dielectric polarization. II. Frequency domain studies of gating currents. *J. Gen. Physiol.* 79:41–67.

Fishman, H. M. 1973. Low-impedance capillary electrode for wide-band recording of membrane potential in large axons. *IEEE (Inst. Electr. Electron. Eng.) Trans. Biomed. Eng.* 20:380–382.

Fishman, H. M. 1982. Current and voltage clamp techniques. *In* Techniques in Cellular Physiology P. F. Baker, editor, Elsevier/North Holland Biomedical Press, Amsterdam. P119:1–42.

Fishman, H. M., D. J. M. Poussart, and L. E. Moore. 1975*a*. Noise measurements in squid axon membrane. *J. Membr. Biol.* 24:281–304.

Fishman, H. M., L. E. Moore, and D. J. M. Poussart. 1975*b*. Potassium-ion conduction noise in squid axon membrane. *J. Membr. Biol.* 24:305–328.

Fishman, H. M., L. E. Moore, and D. J. M. Poussart. 1977. Ion movements and kinetics in squid axon. II. Spontaneous electrical fluctuations. *Ann. NY Acad. Sci.* 303:399–423.

Fishman, H. M., D. Poussart, and L. E. Moore. 1979. Complex admittance of Na conduction in squid axon. *J. Membr. Biol.* 50:43–63.

Fishman, H. M., L. E. Moore, and D. Poussart. 1981. Squid axon K conduction: admittance and noise during short- versus long-duration step clamps. *In* The Biophysical Approach to Excitable Membranes. W. J. Adelman, Jr. and D. E. Goldman, editors. Plenum Publishing Corp., New York. 65–95.

Fishman, H. M., H. R. Leuchtag, J. Sanchez, and L. E. Moore. 1982. Comparison of noise and admittance data in squid axon indicates nonlinearity in Na channel kinetics. *Biophys. J.* 37(2, Pt. 2):102*a*. (Abstr.)

Frehland, E. 1980. Current fluctuation in discrete transport systems far from equilibrium. Breakdown of the fluctuation-dissipation theorem. *Biophys. Chem.* 12:63–71.

Frehland, E. 1982. Stochastic processes—Applications to fluctuations in biological transport systems. *In* Lecture Notes in Biomathematics. Springer-Verlag New York, Inc., New York. In press.

Frehland, E., and K. H. Faulhaber. 1980. Nonequilibrium ion transport through pores. The influence of barrier structures on current fluctuations, transient phenomena, and admittance. *Biophys. Struct. Mech.* 7:1–16.

Gupta, M. S. 1982. Thermal noise in nonlinear resistive devices and its circuit representation. *Proc. IEEE.* 70:788–804.

Hodgkin, A. L., A. F. Huxley, and B. Katz. 1952. Measurement of current-voltage relations in the membrane of the giant axon *Loligo. J. Physiol. (Lond.).* 116:424–448.

Kubo, R. 1957. Statistical-mechanical theory of irreversible processes. I. General theory and simple applications to magnetic and conduction problems. *J. Physiol. Soc. Jpn.* 12:570–586.

Leuchtag, H. R., H. M. Fishman, and D. Poussart. 1982. Osmotic-shock effects on the impedance and voltage-clamp currents of squid axon. *Biophys. J.* 37 (2, Pt. 2):257*a*. (Abstr.)

Marmont, G. 1949. Studies on the axon membrane. I. A new method. *J. Cell. Comp. Physiol.* 34:351–382.

Moore, L. E., H. M. Fishman, and D. J. M. Poussart. 1979. Chemically induced K^+ conduction noise in squid axon. *J. Membr. Biol.* 47:99–112.

Neher, E., and C. F. Stevens. 1977. Conductance fluctuations and ionic pores in membranes. *Annu. Rev. Biophys. Bioeng.* 6:345–381.

Nyquist, H. 1928. Thermal agitation of electric charge in conductors. *Physiol. Rev.* 32:110–113.

Poussart, D., and U. S. Ganguly. 1977. Rapid measurement of system kinetics, an instrument for real-time transfer function analysis. *Proc. IEEE.* 65:741–747.

Poussart, D., L. E. Moore, and H. M. Fishman. 1977. Ion movements and kinetics in squid axon. I. Complex admittance. *Ann. NY Acad Sci.* 303:355–379.

Sigworth, F. J. 1977. Sodium channels in nerve apparently have two conductance states. *Nature (Lond.).* 270:265–267.

Taylor, R. E., C. M. Armstrong, and F. Bezanilla. 1976. Block of sodium channels by external calcium ions. *Biophys. J.* 16(2, Pt. 2):27*a*. (Abstr.)

van Kampen, N. G. 1969. Thermal fluctuations in nonlinear systems. *In* Advances in Chemical Physics, Vol. 15, Stochastic Processes in Chemical Physics. K. E. Shuler, editor. John Wiley & Sons, Inc., New York, 65–77.

Yamamoto, D., J. Z. Yeh, and T. Narahashi. 1982. Current-voltage relationships of single sodium channels in neuroblastoma cells. *Biophys. J.* 41(2, Pt. 2):51*a*. (Abstr.)